2nd Mediterranean Conference on Fracture and Structural Integrity

Fracture simulation of viscoelastic membranes by ordinary state-based peridynamics

M. Ozdemir[a,b,*], S. Oterkus[a], E. Oterkus[a], I. Amin[a,c], A. El-Aassar[d], H. Shawky[d]

[a]*Department of Naval Architecture, Ocean and Marine Engineering, University of Strathclyde, Glasgow G4 0LZ, United Kingdom*
[b]*Department of Naval Architecture and Marine Engineering, Ordu University, Fatsa/Ordu 52400, Turkey*
[c]*Department of Naval Architecture and Marine Engineering, Port Said University, Port Said 42526, Egypt*
[d]*Egypt Desalination Research Center of Excellence (EDRC) and Hydrogeochemistry Department, Desert Research Centre, Cairo 11753, Egypt*

Abstract

Despite a load below the elastic limit is applied on a viscoelastic material, the material may fail after a long duration of constant loading because of the time-dependent viscous deformations. In this regard, a viscoelastic material model in the ordinary state-based peridynamic framework is proposed to capture crack propagation in polymeric water treatment membranes. The deformation state is decoupled into dilatational and distortional parts, and it is assumed that the dilatational part of deformation is elastic, while the distortional part is considered as viscoelastic, whose behaviour can be represented by the Prony series. First, we verify our implementation with FEM results for a benchmark case. Afterwards, the crack propagation is studied by the viscoelastic ordinary state-based peridynamic model.

Keywords: peridynamics; cracks; viscoelasticity; membranes

1. Introduction

The impact of climate change on earth has been causing scarcity of the water resources all around the world, see the United Nations report for an extensive work on the impacts of climate change, UN climate change (2022). Especially, the societies, who live in geographically disadvantageous areas, are expected to suffer from water scarcity further in the near future. In this regard, it is crucial not only to protect available water resources but also to reuse of the waste-water for a sustainable resource management.

In water treatment systems, the membrane materials can be basically categorized as organic or inorganic Baker (2004). The mechanical properties of organic membranes can be improved further by composing with some inorganic compounds as exemplified by Madaeni et al. (2015).

---

* Corresponding author
  E-mail address: murat.ozdemir@strath.ac.uk

Nomenclature

δ	horizon radius of a particle
$\underline{e}$	extension state between two particles
$\underline{e}^{\text{d}}$	distortional part of the extension state between two particles
$\underline{e}^{\text{de}}$	elastic part of the distortional extension state between two particles
$\underline{e}^{\text{vis}}$	viscous part of the extension state between two particles
$\mathcal{H}$	domain of neighbourhood, also called horizon
k′	PD constant related to the bulk modulus
λ	PD constant related to the shear modulus
μ	step function that defines the bond condition
$\underline{\omega}$	scalar state of the weight function
φ	local damage parameter of a particle
q	weighted volume of the horizon for a particle
ρ	density of the material
t	force density vector
t^{d}	distortional part of the force density
t^{k}	dilatational part of the force density
τ_i	relaxation time for each Maxwell element in the Prony series
θ	PD volume dilatation
V	volume of a material point

The main constituent of the organic based membranes are polymers, which naturally demonstrate some degree of viscous deformations even at the room temperature, Chung et al. (2000). The viscoelastic properties of the membrane materials can be identified by either dynamic mechanical analysis, see Chartoff et al. (2008) or tensile creep tests with the load levels below the elastic limit, see Emori et al. (2019).

Mechanical characterization of membrane materials used in waste-water treatment systems can be performed by several methods of which many of them are also common in other engineering applications, e.g, civil and structural engineering. These techniques were summarized for various membrane materials by Wang et al. (2017).

Despite the operation load, which is below the critical level based on static analysis approach, the deformations in viscoelastic membranes tend to increase by time. This effect becomes prominent if the temperature of working environment is higher than the glass transition temperature of the material. Chung et al. (2000) showed the influence of temperature on the viscous behaviour of polymeric water treatment membranes. Considering this phenomenon, it is required to predict the long-term response of a polymeric membrane under given loading conditions. In this particular study, we therefore examine the growth of an existing crack and full failure of the membrane due to the viscous deformations under constant loads.

The modelling of defects is inherently a challenging task when conventional continuum mechanics based methods are employed. However, the damage evolution and crack propagation can be numerically simulated by a recent methodology, called as peridynamics (PD), which was proposed by Silling (2000). The simplest form of the PD is bond-based approach, which defines the force interaction solely depending on the relative deformation of the particles, Silling and Askari (2005). The bond-based PD hence introduces some limitations on the material constants. A more comprehensive PD approach, which is called ordinary state-based (OSB) PD was later proposed by Silling et al. (2007).

A simplified form of OSB-PD was presented by Le et al. (2014) for two-dimensional (2D) plane stress and plane strain cases by correspondence of the strain energy densities and volume dilatations in classical and PD theories. The 2D OSB-PD formulation presented by Le et al. (2014) was adopted by Ozdemir et al. (2020) for the dynamic crack-propagation simulation in functionally graded materials. Then, a comprehensive investigation on the micro-macro crack interactions in functionally graded materials employing the same formulation was carried out by Ozdemir et al. (2022).

The outstanding features of OSB-PD have been adopted for material simulations, which involve nonlinear effects. Madenci and Oterkus (2016) decomposed the deformation states of materials into dilatational and distortional parts, and proposed OSB-PD formulation for plastic deformations with von-Mises yielding criterion and isotropic hardening. Being able to decompose the deformation states in OSB-PD perspective has enabled the researchers to introduce viscoelastic effects in the PD models, see for example Mitchell (2011); Madenci and Oterkus (2017).

In the light of the works by Mitchell (2011) and Madenci and Oterkus (2017), we introduce viscous deformation effects into the 2D plane stress OSB-PD formulation in the present work. The rest of the present work is outlined as follows. In Section 2, we will present 2D viscoelastic OSB-PD formulation for the plane stress case. Section 3 will be covering the verification of the proposed formulation with the viscoelastic FEM analysis using a commercial FE code, Ansys (2020). Afterwards, the crack propagation simulations of the viscoelastic membranes will be carried out in Section 4. The concluding remarks will be drawn in Section 5.

2. OSB-PD Formulation for Viscoelastic Deformations

2.1. Fundamentals

In the PD framework, we basically solve the equation of motion in the discretized domain. The discrete form of the equation of motion can be written as:

$$\rho\ddot{\mathbf{u}}_{(k)} = \sum_{j=1}^{N_{\mathcal{H}_k}} (\mathbf{t}_{(k)(j)} - \mathbf{t}_{(j)(k)})V'_{(j)} + \mathbf{b}_{(k)}. \tag{1}$$

In Eq. (1), the force density vectors are denoted as $\mathbf{t}_{(k)(j)}$ and $\mathbf{t}_{(j)(k)}$ between the particles (k) and (j) within the horizon of particle (k). The number of particles in the neighbourhood of particle (k) is represented by $N_{\mathcal{H}_k}$. The displacement and acceleration vectors are expressed by $\mathbf{u}$ and $\ddot{\mathbf{u}}$, respectively. The remaining parameters in Eq. (1) are: ρ, V' and $\mathbf{b}$, which respectively stand for the density of material, corrected volume for the particles and the body force density vector.

In the present study, we adopt 2D OSB-PD formulation from the work by Le et al. (2014). The force density for linear elastic solids can be expressed as:

$$t = \frac{2(2\nu - 1)}{\nu - 1}\left(k'\theta - \frac{\lambda}{3}(\underline{\omega e^d}) \bullet \underline{x}\right)\frac{\omega x}{q} + \lambda\underline{\omega e^d}. \tag{2}$$

In the force density expression, ν stands for the Poisson's ratio; k' and λ represent the PD material constants for the dilatational and distortional parts of deformation, respectively. These constants can be obtained by the correspondence of volumetric dilatations and strain energy densities in the PD and classical theory. The symbol "•" denotes the dot product of two PD states, see Silling et al. (2007) for details. The volume dilatation, θ for the plane stress condition can be written as:

$$\theta = \frac{2(2\nu - 1)}{\nu - 1}\frac{(\underline{\omega x}) \bullet \underline{e}}{q}, \tag{3}$$

The parameter $\underline{\omega}$ is scalar state of the weight function, and it is expressed as $\underline{\omega} = 1 - \underline{x}/\delta$ with the horizon radius δ and the initial distance between the particles, $\underline{x}$. The parameter q represents the weighted volume of the horizon for each particle, and it is defined as $q = (\underline{\omega x}) \bullet \underline{x}$.

2.2. Viscous deformations

In order to introduce viscous deformations, we firstly decompose the force density into dilatational and distortional parts as $t = t^k + t^d$ Madenci and Oterkus (2016). Here, the dilatational part of the force density is identical for both linear elastic and viscoelastic solids, and is given as follows.

$$t^k = \frac{2(2\nu - 1)}{\nu - 1}k'\theta\frac{\omega x}{q}. \tag{4}$$

Then, by the assumption of incompressibility in viscous fluids, only the distortional part of the deformation is split into elastic and viscous parts, i.e., $\underline{e}^{d} = \underline{e}^{de} + \underline{e}^{vis}$.

It is a common practice to represent viscoelastic properties by means of general Maxwell models, in which a single spring element is connected with a series of parallel Maxwell elements. The constitutive relation for the general Maxwell model is represented by the Prony series Lakes (2009). The Prony series basically represent the relaxation of the material, which results in either continuous deformation under constant loading or stress release under constant deformations with respect to time. In the PD perspective, the parameter λ is the time dependent material property, and can be expressed by the Prony series as follows.

$$\lambda(t) = \lambda_{\infty} + \sum_{i=1}^{N_M} \lambda_{(i)} e^{-t/\tau_i}, \tag{5}$$

where τ_i represents the relaxation time for each Maxwell element. The limit value of the material constant as the time converges to infinity is λ_{∞}. The number of Maxwell elements in the general Maxwell model is denoted by N_M.

In a general Maxwell model, the distortional part of the force density is expressed as:

$$t^{d} = t_{\infty}^{d} + \sum_{i=1}^{N_M} t_{(i)}^{d}, \tag{6}$$

where t_{∞}^{d} stands for the distortional part of force density for the single spring element, while the distortional force density component acting on each Maxwell element is denoted by $t_{(i)}^{d}$. Considering the viscous deformations, the force density expression for each Maxwell element is obtained as:

$$t_{(i)}^{d} = \lambda_{(i)} \underline{\omega} \left(\underline{e}^{d} - \underline{e}_{(i)}^{vis} \right) - \frac{2(2\nu-1)}{(\nu-1)} \left[\lambda_{(i)} \underline{\omega}(\underline{e}^{d} - \underline{e}_{(i)}^{vis}) \bullet \underline{x} \right] \frac{\underline{\omega x}}{q} \tag{7}$$

By substituting Eq. (7) into Eq. (6), the distortional part of the force density in a general Maxwell model can be expressed as:

$$t^{d} = \lambda \underline{\omega} \underline{e}^{d} + \frac{2(2\nu-1)}{(\nu-1)} \left[\lambda(\underline{\omega} \underline{e}^{d}) \bullet \underline{x} \right] \frac{\underline{\omega x}}{q} - \frac{2(2\nu-1)}{(\nu-1)} \sum_{i=1}^{N_M} \left[\lambda_{(i)}(\underline{\omega} \underline{e}_{(i)}^{vis}) \bullet \underline{x} \right] \frac{\underline{\omega x}}{q} - \sum_{i=1}^{N_M} \lambda_{(i)} \underline{\omega} \underline{e}_{(i)}^{vis}. \tag{8}$$

The viscous extension state $\underline{e}^{vis}$ at each time increment can be obtained according to the procedure described by Mitchell (2011).

2.3. Damage representation

The inclusion of damage and structural discontinuities in the PD formulation is rather straightforward. The interactions between the particles can be removed irreversibly to generate a damaged region. The damage accumulation in a PD particle is quantified by the local damage parameter φ as follows Silling and Askari (2005).

$$\varphi(\mathbf{x}) = 1 - \frac{\int_{\mathcal{H}_x} \mu(\mathbf{x}, \xi) d\mathcal{H}}{\int_{\mathcal{H}_x} d\mathcal{H}}, \tag{9}$$

where the step function $\mu(\mathbf{x}, \xi)$ represents the bond condition between the particle located at $\mathbf{x}$ and its neighbour, and takes the value of 1.0 for the intact bonds, and zero for the broken bonds. ξ defines the bond vector between the particles.

There are several criteria to assess the bond condition in the PD perspective, and some of them have been covered by Dipasquale et al. (2017). The most common one is the so called critical stretch criterion, which was clearly defined for bond-based PD by Silling and Askari (2005), and defined for OSB-PD in Madenci and Oterkus (2014). Despite the implementation of critical stretch criterion is rather straightforward, its validity is limited to linear elastic problems. Since the present problem involves non-linearities arising from the viscous part of the deformation, the critical bond

(a)

$E = 16600$ MPa
$\rho = 1810$ kg/m^3
$\nu = 0.3$
$\sigma_0 = 2000$ Pa

$W = 0.15$ m

$L = 0.3$ m
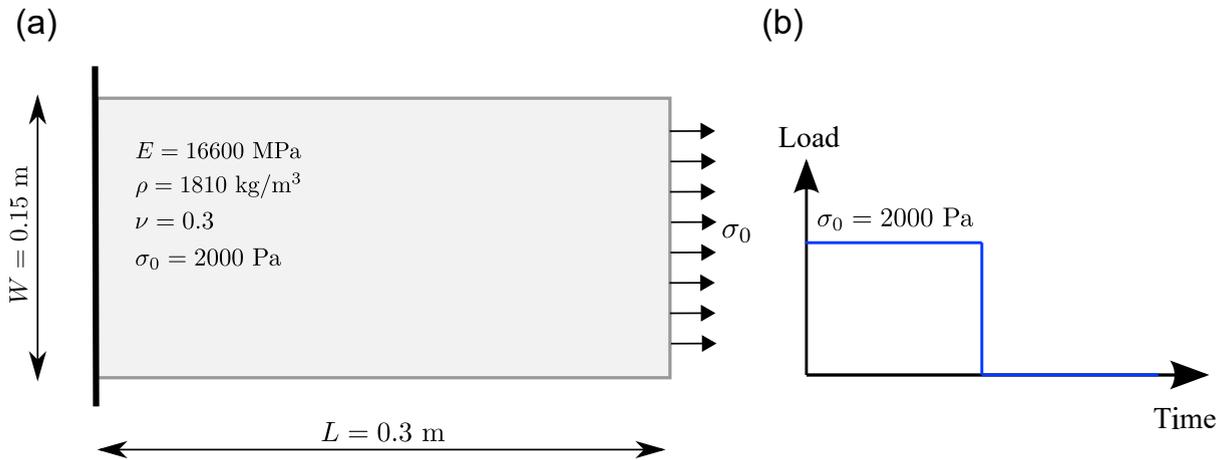
σ_0

(b)

Load

$\sigma_0 = 2000$ Pa

Time

Fig. 1. Benchmark problem for uniaxial tension specimen: (a) representative model, (b) loading condition.

strain energy density criterion by Foster et al. (2011) is employed to examine the bond conditions. The critical value of the strain energy density that can be stored in a bond for a 2D case was given by Dipasquale et al. (2017) as follows.

$$\Gamma_c = \frac{3G_c}{2\delta^3 t_h},$$ (10)

where G_c stands for the critical energy release rate of the material, whereas t_h is the thickness of 2D model. If the strain energy density of a bond exceeds the value given by Eq. (10), the step function is set to zero for the associated bond, i.e., $\mu(\mathbf{x}, \xi) = 0$. Then, the weight function ω is multiplied by the step function in the force density and dilatation expressions.

3. Numerical Studies

The solution of the PD equation of motion can be performed by an explicit time integration scheme. However, the present work requires extra care when dealing with the time integration. The steps for solving the viscoelastic PD models were given by Madenci and Oterkus (2017). The problem itself is transient, which means that the viscous deformations are to be updated for each real time increment. However, for each real time increment, it is required to evaluate almost steady-state displacement field by employing the adaptive dynamic relaxation (ADR) technique in a virtual time frame, see Kilic and Madenci (2010) and Madenci and Oterkus (2014) for the implementation of ADR in the PD perspective.

3.1. Verification of the OSB-PD formulation

In the verification stage of our OSB-PD viscoelastic formulation, we simply consider flat-sheet type polymeric specimen under uniaxial tensile load, which was previously studied by Madenci and Oterkus (2017). The problem is described in Fig. 1.

The fundamental material properties are indicated in Fig. 1(a); however, these properties represent the material response at the initial stage. We can expect the relaxation of the modulus of elasticity as the time passes. The material relaxation is thus represented by the Prony series invoking 15 terms. The parameters of the Prony series are adopted from Madenci and Oterkus (2017), and are given in Table 1. In the given table, E_∞ stands for the modulus of elasticity when the time converges to infinity, which means the material modulus will relax from 16600 MPa to 700 MPa in an exponential manner.

A step loading, as shown in Fig. 1(b), is applied to the right edge of the model while keeping the left edge fixed. A uniform tension load of magnitude $\sigma_0 = 2000$ Pa is suddenly applied on the loaded edge for 5 ms, then the load is removed. Total time of the simulation is set as 10 ms.

In order to capture the material relaxation accurately, the time increment size is adopted as $\Delta t = 1 \times 10^{-4}$ s. As stated previously, the steady-state displacement field is obtained by the ADR algorithm. As for the comparison purposes, transient dynamic analysis was performed by a commercial FE code, Ansys (2020). In both FEM and PD simulations, the domain discretization is performed by 100×50 elements/particles. The thickness of the model is assumed to be $L/100$. Plane182 element with plane stress formulation is employed by considering the full integration of the stiffness matrix in Ansys.

The displacement histories of the loaded edge by FEM and OSB-PD have been recorded, and compared in Fig. 2. The given figure suggests that the proposed OSB-PD formula is capable of capturing the creep deformation of the membrane in the time interval of 0-5 ms. Beyond the load release point, the membrane starts to recover its original shape. The recovery of the membrane has also been captured by OSB-PD with a good accuracy.

3.2. Crack propagation cases

We have verified our OSB-PD formulation for a viscoelastic membrane under uniaxial tensile loading in section 3.1. The crack propagation cases can be simulated next.

In the crack propagation simulations, the main dimensions and the material properties are the same with those in section 3.1; however, an angular crack is introduced in the centre of the membrane. The magnitude of the load is chosen so that the membrane keeps structural integrity at the beginning, yet the failure takes place in a reasonable period by the relaxation of the membrane. The cracked membrane specimen and its loading condition are depicted in Fig. 3.

A series of parametric analyses was performed by varying the crack orientation angle with respect to the horizontal axis, i.e., $\theta = 30°$, $45°$ and $90°$. The crack patterns at the instance just before the failure and at the intance of full failure were given in Fig. 4. These failure patterns obviously indicate the mode-I type failure under uniaxial tension for all crack orientations.

As expected, the crack orientation angles have significantly influenced the full failure time. When the crack is perpendicular to the loading direction, i.e., $\theta = 90°$, the specimen fails after 0.05 ms. The full failure time for $\theta = 45°$ is 5.3 ms. However, when the crack orientation is set as $\theta = 30°$, the full failure time becomes 5.6 s, which is a dramatic increase of the time until the full failure. In case of $\theta = 30°$ specimen, the full failure takes place at a relatively late stage compared to the other crack orientations cases; therefore, it is required to adjust the time step size properly. For instance, the simulations can be conducted with a relatively small time increment, $\Delta t = 1 \times 10^{-4}$ s, at the beginning. Then, it can be adjusted, e.g., $\Delta t = 1 \times 10^{-1}$ s, for achieving the required failure time in a computationally efficient way.

Table 1. Prony series parameters for the material from Madenci and Oterkus (2017).

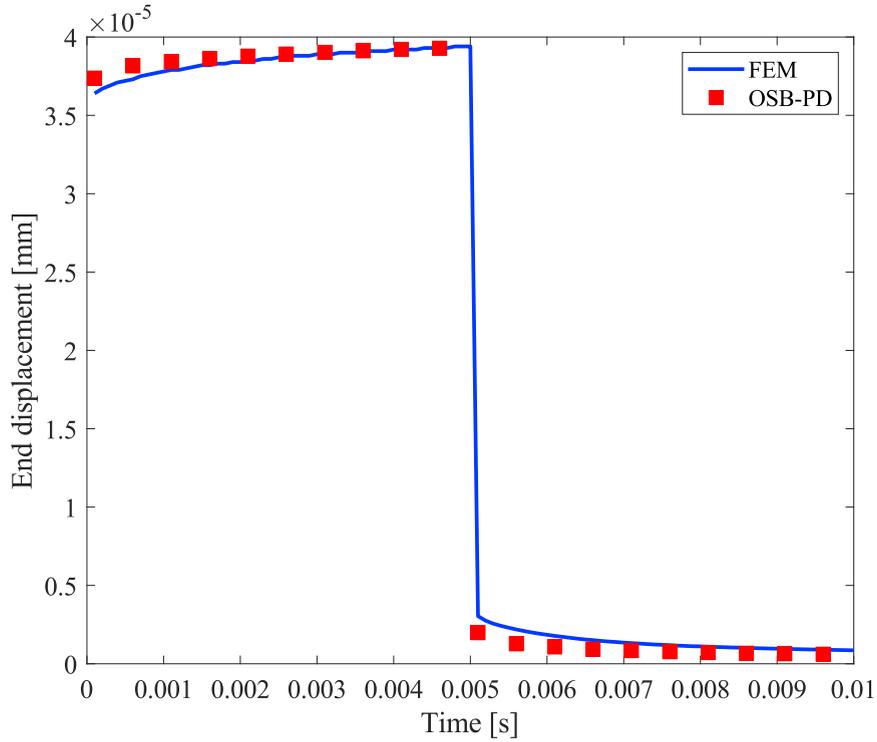| i	τ_i	E_i [MPa]
1	1.0E-4	200
2	1.0E-3	800
3	1.0E-2	1500
4	1.0E+0	1000
5	1.0E+1	1100
6	1.0E+2	2700
7	1.0E+3	2900
8	1.0E+4	2500
9	1.0E+5	900
10	1.0E+6	950
11	1.0E+7	600
12	1.0E+8	120
13	1.0E+9	180
14	1.0E+11	200
15	3.0E+12	250
	E_∞	700

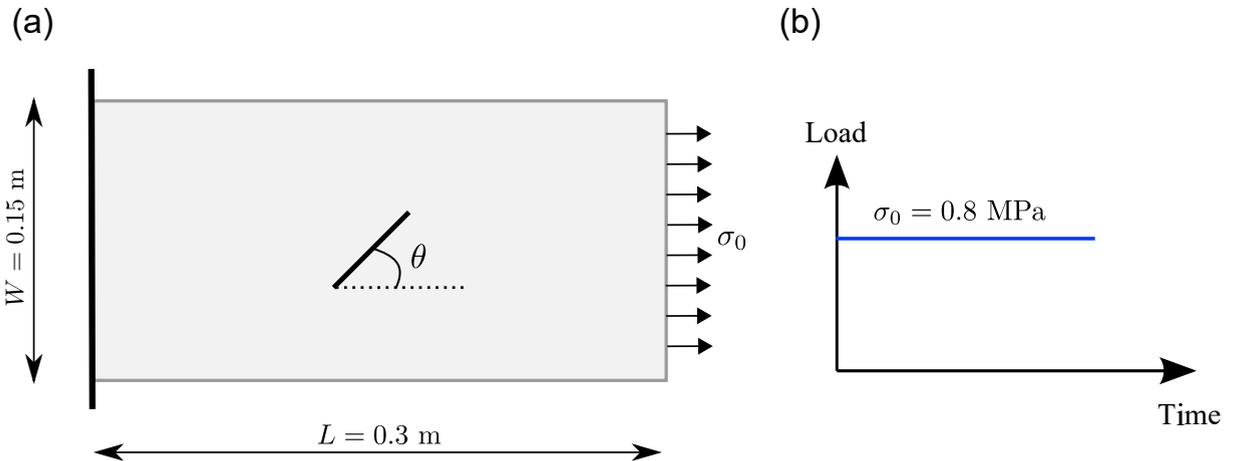Fig. 2. Loaded edge displacement history of the flat-sheet membrane under uniaxial loading.

Fig. 3. Cracked membrane specimen: (a) modelling, (b) loading condition.

The end displacement history for $\theta = 30°$ case has been extracted and presented in Fig. 5. This figure suggests that a significant portion of the creep deformation takes place within a very short time, e.g., 1.0 s due to the exponential form of the relaxation terms in the Prony series. Beyond 1.0 s, the displacement increment rate is quite small compared to the first 1.0 s. After 5.5 s, the sudden increase of the displacement is the evidence for full failure of the specimen.
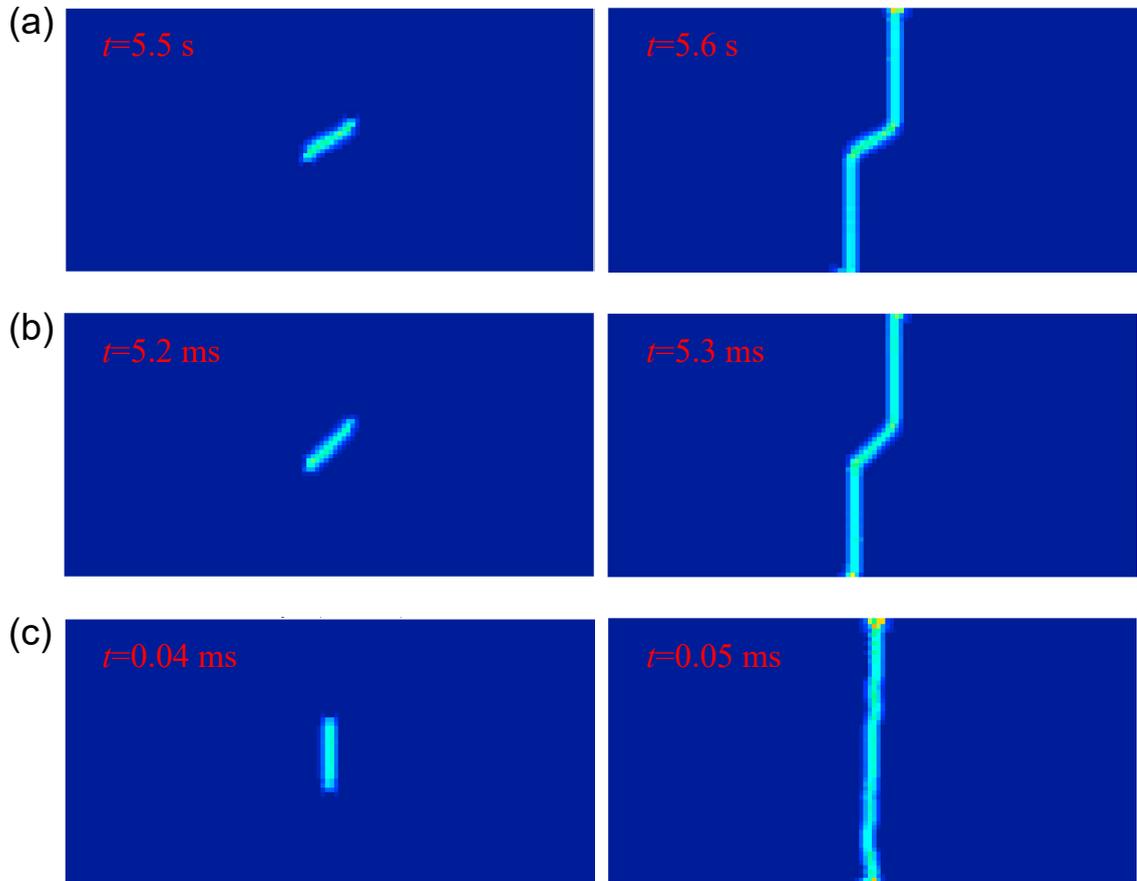
Fig. 4. Damage patterns for viscoelastic membranes with various crack orientation angles: (a) $\theta = 30°$, (b) $\theta = 45°$, (c) $\theta = 90°$.

4. Concluding Remarks

The viscoelastic deformation of the polymeric membranes has been highlighted. Then, the numerical representation of material relaxation by the Prony series was articulated, and this approach was employed in both our OSB-PD formulation and the commercial FE code. By the comparison of FE and OSB-PD displacements for the membrane sheet, we demonstrated the validity of our formulation for the viscoelastic deformations. Once present model had been verified, the crack propagation simulations were performed to examine the influence of crack orientation angle and the time dependent material response. It was found that the crack orientation angle has a prominent impact on the time period until the full failure.

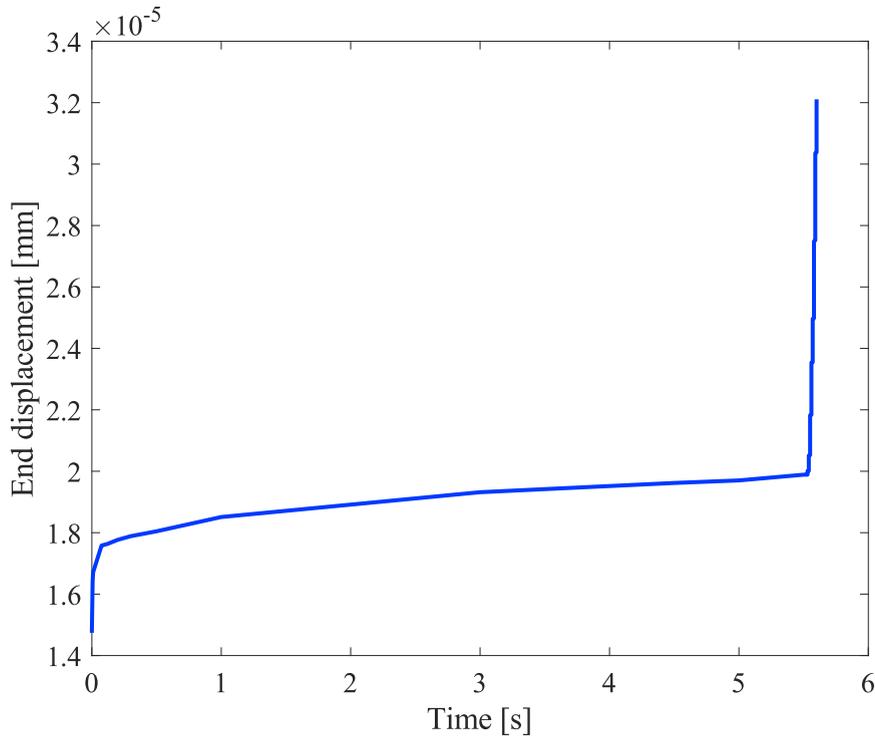Fig. 5. Displacement history of the loaded edge for $\theta = 30°$ case.

References

ANSYS Mechanical APDL structural analysis guide, 2020. ANSYS Inc, Canonsburg PA.

Baker, R.W., 2004. *Membrane technology and applications.* 2nd edn. John Wiley & Sons, West Sussex.

Chartoff, R.P., Menczel, J.D., Dillman, S.H., 2008. Dynamic mechanical analysis (DMA). In: Thermal Analysis of Polymers. John Wiley & Sons, New Jersey, pp. 387–495.

Chung, T.S., Qin, J.J., Gu, J., 2000. Effect of shear rate within the spinneret on morphology, separation performance and mechanical properties of ultrafiltration polyethersulfone hollow fiber membranes. Chemical Engineering Science 55, 1077-1091.

Climate change, 2022. Impacts, adaptation and vulnerability, summary for policy makers. United Nations.

Dipasquale, D., Sarego, G., Zaccariotto, M., Galvanetto, U., 2017. A discussion on failure criteria for ordinary state-based peridynamics. Engineering Fracture Mechanics 186, 378-398.

Emori, K., Miura, T., Kishida, H., Yonezu, A., 2019. Creep deformation behavior of polymer materials with a 3D random pore structure: Experimental investigation and FEM modeling. Polymer Testing 80, 106097.

Foster, J.T., Silling, S.A., Chen, W., 2011. An energy based failure criterion for use with peridynamic states. International Journal for Multiscale Computational Engineering 9, 675–688.

Kilic, B., Madenci, E., 2010. An adaptive dynamic relaxation method for quasi-static simulations using the peridynamic theory. Theoretical and Applied Fracture Mechanics 53, 194–204.

Lakes, R., 2009. *Viscoelastic materials.* Cambridge University Press, New York.

Le, Q.V., Chan, W.K., Schwartz, J., 2014. A two-dimensional ordinary, state-based peridynamic model for linearly elastic solids. International Journal for Numerical Methods in Engineering 98, 547-561.

Madaeni, S.S., Ghaemi, N., Rajabi, H., 2015. Advances in polymeric membranes for water treatment. In: Basile, A., Cassano, A., Rastogi, N.K. (eds.) Advances in membrane technologies for water treatment: Materials, processes and applications. Woodhead Publishing, Cambridge, pp. 3-41.

Madenci, E., Oterkus, E., 2014. *Peridynamic theory and its applications.* Springer, New York.

Madenci, E., Oterkus, S., 2016. Ordinary state-based peridynamics for plastic deformation according to von Mises yield criteria with isotropic hardening. Journal of the Mechanics and Physics of Solids 86, 192–219.

Madenci, E., Oterkus, S., 2017. Ordinary state-based peridynamics for thermoviscoelastic deformation. Engineering Fracture Mechanics 175, 31–45.

Mitchell, J.A., 2011. A non-local, ordinary-state-based viscoelasticity model for peridynamics. SAND2011-8064. Albuquerque: Sandia National Laboratories.

Ozdemir, M., Imachi, M., Tanaka, S., Oterkus, S., Oterkus, E., 2022. A comprehensive investigation on macro–micro crack interactions in functionally graded materials using ordinary-state based peridynamics. Composite Structures 287, 115299.

Ozdemir, M., Kefal, A., Imachi, M., Tanaka, S., Oterkus, E., 2020. Dynamic fracture analysis of functionally graded materials using ordinary state-based peridynamics. Composite Structures 244, 112296.

Silling, S.A., 2000. Reformulation of elasticity theory for discontinuities and long-range forces. Journal of the Mechanics and Physics of Solids 48, 175-209.

Silling, S.A., Askari, E., 2005. A meshfree method based on the peridynamic model of solid mechanics. Computers & Structures 83, 1526-1535.

Silling, S.A., Epton, M., Weckner, O., Xu, J., Askari, E., 2007. Peridynamic states and constitutive modeling. Journal of Elasticity 88, 151-184.

Wang, K., Abdalla, A.A., Khaleel, M.A., Hilal, N., Khraisheh, M.K., 2017. Mechanical properties of water desalination and wastewater treatment membranes. Desalination 401, 190–205.